In-situ pressureless sintering MgAlON-MgO ceramic from spent MgO-C brick towards friction material and refractory applications

Xiang Cheng
University of Science and Technology Beijing
Xiwang Miao
University of Science and Technology Beijing
Lei Liu
University of Science and Technology Beijing
Ying Zhang
University of Science and Technology Beijing
Min Guo
University of Science and Technology Beijing
Fangqin Cheng
Shanxi University
Mei Zhang (zhangmei@ustb.edu.cn)
University of Science and Technology Beijing

Research Article

Keywords: Spent MgO-C brick, MgAlON-MgO, Friction material, Refractory, Impurity

Posted Date: March 18th, 2021

DOI: https://doi.org/10.21203/rs.3.rs-332049/v1

Abstract

MgAlON-MgO ceramic was in-situ synthesized at 1600℃ from spent MgO-C brick by pressureless sintering towards friction material and refractory applications, respectively. The flexural strength of MgAlON-MgO ceramic reaches as high as 172MPa with 11.1% utilization ratio of spent MgO-C brick. Moreover, MgAlON-MgO ceramic still has a good flexural strength up to 46MPa when utilization ratio of spent MgO-C brick increases to 52.9%. The impurities introduced by the spent brick distribute in MgAlON-MgO ceramic in the form of $CaMgSiO_4$ and $MgFe_2O_4$. $CaMgSiO_4$ increases the density of MgAlON-MgO ceramic and subsequently enhance its flexural strength, while $MgFe_2O_4$ has no more obvious effect on those of the ceramic. Hence, MgAlON-MgO ceramic with different strength can be controllably prepared by simply adjusting utilization ratio of spent MgO-C brick, which maybe use as the friction material and refractory.

1. Introduction

With the development of automobile industry, the performance requirements of automobile brake friction material are getting even strict[1]. Ceramic-based friction materials are widely used in automobile brake blocks due to their high thermal and abrasion resistance, excellent mechanical strength, light wight[2]. The common ceramic-based friction materials mainly include short carbon fiber reinforced silicon carbide (Csf/SiC) composite material, carbon fiber reinforced carbon-silicon carbide dual matrix (C/C-SiC) composite material and so on[3–5]. Yang et al.[6] prepared C/C-SiC composite material by twice hot-press curing at 120℃ and 180℃, pyrolysising at 1000℃ and liquid phase silicon filtration (LSI) process preforming at 1450℃. Tang et al.[7] have synthesized Csf/SiC composite material at 1800℃ by hot-press sintering under flowing argon atmosphere using Si powder as sintering aid. Hence, application of ceramic-based friction material is limited because its complex synthesis process and high production cost.

Magnesium aluminium oxynitride (MgAlON) is a kind of spinel formed from the solid solution reaction of AlN, Al_2O_3 and MgO[8], which is a candidate for used as friction material due to it has excellent mechanical strength, high temperature stability and so on[9–11]. Nevertheless, the application of MgAlON is inhibited because of the high production cost of MgAlON, which is normally prepared by hot-pressing technology. Hence, MgAlON based ceramic prepared by pressureless sintering has attracted the attention of scholars. For instance, Cheng et al.[12] obtained MgAlON bonded MgO composite material at 1450℃ for 5h by using aluminium powder, Al_2O_3 powder and fused magnesite as raw materials, and pointed out that the compressive strength of the material reached 43MPa. Yang et al.[13] prepared MgAlON-MgO composite material by aluminothermy reduction method under flowing nitrogen atmosphere at 1500℃ for 6 hours, its compressive strength and flexural strength were 53 and 10 MPa, respectively. However, mechanical property of MgAlON-MgO composite ceramic from pressureless sintering in those researches was too poor to meet the requirement of friction material. Wang et al.[14] pointed out that stress cracks were generated to damage the mechanical strength of the MgAlON bonded

MgO composite material in the sintering process of material due to the large difference of thermal expansion coefficient between MgO ($13\times10^{-6}\ ℃^{-1}$) and MgAlON ($\sim 7.4\times10^{-6}\ ℃^{-1}$). So, the mechanical strength of the MgAlON-MgO ceramic must be improved by enhancing interfacial binding force between MgAlON and MgO phases.

A large number of refractory materials are consumed every year in high temperature industries such as steel, cement, and glass production. In recent years, the annual output of refractory materials has exceeded 20 million tons in China, generating more than 10 million tons spent refractories each year[15, 16]. Hence, the spent refractory is a typical industrial solid waste that cannot be ignored. The magnesia-carbon (MgO-C) brick is widely used as lining materials for electric furnaces, converters and refining furnaces due to its high thermal conductivity, excellent slag resistance and thermal shock resistance[17]. However, the corrosive effect of steel slag on MgO-C brick during long-term service produces a great number of spent MgO-C bricks that cannot meet the harsh service environment of the furnace lining again. Due to abundant storage of spent MgO-C brick pollutes groundwater and destroys ecological environment while contains precious magnesium and carbon sources, its reutilization has been widely researched. Arianpour et al.[18] used the pre-treated spent MgO-C brick as aggregate to produce magnesia refractory brick and the utilization ratio of spent brick reached 30%. Avelar et al.[19] used slag conditioning additive produced from spent MgO-C refractories to adjust the foaming behavior of electrical arc furnace slag by controlling the MgO content in the slag, while the addition amount of spent MgO-C refractories was 28.57%. Generally, the magnesium source in the spent MgO-C brick was reutilized while ignoring the carbon source, with lower addition amount of spent MgO-C brick. So, in order to make full use of the magnesium source and carbon source in spent MgO-C brick, the spent brick may be adopted for synthesis of MgAlON-MgO composite material by carbothermal reduction and nitridation process. However, the impurities such as Al_2O_3, CaO, SiO_2 and Fe_2O_3 in spent MgO-C brick can't be ignored anymore. Considering the complex chemical composition of spent MgO-C brick, the mechanical properties of the MgAlON-MgO composite ceramic may not be higher enough to meet the demand of friction material when much spent brick is added. Therefore, the effect of utilization ratio of spent MgO-C brick and impurities on the properties of MgAlON-MgO composite material should be explored.

In this work, MgAlON and MgAlON-MgO ceramics were in-situ pressureless synthesized under flowing nitrogen atmosphere at 1600℃ for 3h by carbothermal reduction and nitridation process, and the spent MgO-C brick was used as raw material, while the mechanical strength of the ceramics was researched. In order to improve the utilization ratio of spent MgO-C brick, the effect of the spent MgO-C brick addition on phase composition, microstructure and mechanical property of the MgAlON-MgO composite material were studied. Finally, the effect of impurity introduced by spent MgO-C brick in the MgAlON-MgO ceramic on the flexural strength of the ceramic was studied.

2. Experimental Procedure

2.1. Raw materials and preparation process

In this research, spent MgO-C brick, alumina micro-powder and fused magnesite were used as raw materials, and 5wt% polyvinyl alcohol (PVA) aqueous solution was used as binder. It was noted that the powder with particle size less than 74μm was selected as raw material after the spent MgO-C brick was crushed. Table 1 lists the chemical composition of the raw materials. As shown in the table, the spent MgO-C brick has complex composition and contains 13.53wt% impurities except for 72.9wt% MgO and 13.57wt% C, such as Al_2O_3, CaO, SiO_2 and Fe_2O_3. Based on the previous thermodynamic study[20], the mass ratio of raw materials is shown in Table 2. The series of A were designed to obtain MgAlON-MgO composite material with the best flexural strength by controlling the addition amount of fused magnesite. And the series of B were designed to improve the utilization ratio of spent MgO-C brick. According to Table 2, the raw materials were accurately weighed and mixed by planetary ball milling with absolute alcohol as medium for 4h. The mixture was pressed at 100MPa by means of uniaxial compression method to form cubic samples of 40×10×6mm. Subsequently, the cuboid samples were dried at 110℃ for 12h. The dried green bodies were placed in a corundum crucible and sintered at 1600℃ for 3h under flowing nitrogen atmosphere.

Table 1
Chemical composition of raw materials

Raw materials	**Chemical composition/wt%**					
	MgO	**Al_2O_3**	**CaO**	**SiO_2**	**Fe_2O_3**	**C**
spent MgO-C brick	72.90	3.30	3.72	4.48	1.37	13.57
alumina micro-powder	-	99.39	-	-	-	-
fused magnesite	95.27	0.31	1.28	2.29	0.57	-

Table 2
Composition of the green bodies

Sample No	Spent MgO-C brick: Alumina micro-powder: Fused magnesite (mass ratio)	Spent MgO-C brick addition (wt%)	Fused magnesite addition (wt%)
A_1	1: 6: 1	12.5%	12.5%
A_2	1: 6: 2	11.1%	22.2%
A_3	1: 6: 3	10.0%	30.0%
A_4	1: 6: 4	9.1%	36.4%
A_5	1: 6: 5	8.3%	41.7%
B_1	1: 6: 2	11.1%	22.2%
B_2	3: 6: 2	27.3%	18.2%
B_3	5: 6: 2	38.5%	15.4%
B_4	7: 6: 2	46.7%	13.3%
B_5	9: 6: 2	52.9%	11.8%

2.2. Characterizations

The diffraction of X-rays (XRD) (MXP21VAHF, Japan) was used to determine the phase composition of samples. The element analysis of raw materials was investigated by X-ray fluorescence spectrometry (XRF) (XRF-1800, Japan) and carbon-sulfur analyzer (EMIA-920V2, Japan), respectively. The field-emission scanning electron microscopy and energy-dispersive spectroscopy (SEM-EDS) (SUPRA55, Germany) was used to observe the fracture morphology and elements distribution of sintered samples. It was noted that surface of the sample should be sprayed with carbon before SEM-EDS analysis. The transmission electron microscope (TEM) (JEM-2200FS, Japan) was used to observe the morphology and determine the existing form of impurity in the composite material. The existence form of nitrogen in the sample was analyzed by X-ray photoelectron spectroscopy (XPS) (AXISULTRA-DLD, Japan). The flexural strength of sample was measured by three-point bending test on an electronic universal testing machine (WDW-100, China). The bulk density of the sample was determined by Archimedes principle. It should be noted that three parallel experiments have be done for each sample to calculate the average value of its flexural strength and bulk density, respectively.

3. Results And Discussion

3.1. Preparation of pure MgAlON

Dai et al.[21] obtained pure MgAlON by carbothermal reduction and nitridation reaction from C, Al_2O_3 and MgO mixture sintering at 1650℃ for 6h with flowing nitrogen atmosphere. So, the similar carbothermal reduction and nitridation process was adopted for preparing pure MgAlON based on the chemical composition of spent MgO-C brick as shown in Table 1. According to the Table 2, sample A_1 was sintered in the flowing nitrogen atmosphere at 1600℃ for 3h using spent MgO-C brick as raw material. Figure 1a reveals the XRD pattern of sintered sample A_1, from which it can be seen that sample A_1 is a spinel phase. Due to magnesia-alumina spinel ($MgAl_2O_4$) and MgAlON have great similar lattice constants and the same crystal structure, the sample A_1 cannot be qualitatively determined by only XRD results. The N 1s XPS spectra of the sample A_1 is shown in Fig. 1b. As observed, there are two obvious peaks where the binding energy is about 395.5eV and 397.9eV, corresponding to the bond of nitrogen atoms with aluminum atoms and oxygen atoms, respectively. According to the XRD and XPS results, pure MgAlON was in-situ synthesized from spent MgO-C brick by pressureless sintering. Figure 1c reveals the fracture morphology of sintered sample A_1. The MgAlON presents an irregular granular shape in the fracture surface, and the particle size is 1–2μm. In addition, the figure shows that the fracture behavior of MgAlON is intergranular fracture.

3.2. Preparation of MgAlON-MgO friction material

Due to the complex chemical composition of spent MgO-C brick corroded by steel slag, containing impurity phases such as CaO, SiO_2 and Fe_2O_3 as shown in Table 1, series of A was designed to in-situ pressureless synthesize MgAlON-MgO composite ceramic by controlling the addition amount of fused magnesite. According to the Table 2, green bodies A_1-A_5 with different fused magnesite addition were sintered at 1600℃ for 3h under flowing nitrogen. Figure 2 shows the XRD patterns of the samples and the relative contents of MgAlON phase and MgO phase in the samples. The relative content was calculated by the reference intensity ratio (RIR) method on the basis of diffraction integral intensity from MgAlON (311) crystal face and MgO (200) crystal face in the XRD results of samples. As shown in Fig. 2a, the MgAlON-MgO composite materials (samples A_2-A_5) were in-situ pressureless synthesized from spent MgO-C brick succesfully. It can be seen from Fig. 2b that the relative content of MgO phase in the samples and growth rate of MgO content increase with the rise of fused magnesite addition.

The fracture morphologies of the specimens A_2-A_5 and the EDS results of specimen A_3 are shown in Fig. 3. By comparing the microscopic morphologies of MgAlON (Fig. 1c) and MgAlON-MgO (Fig. 3a-d), it can be found that the particle size of MgAlON-MgO composite ceramic is larger than that of MgAlON, indicating that the MgO phase may promote the grain growth of MgAlON. Compared with the fracture behavior of MgAlON, the fracture behavior of MgAlON-MgO (A_2) containing 4.2% MgO phase is mainly transgranular fracture accompanied by a few intergranular fractures, manifesting that interfacial binding force between grains of MgAlON-MgO composite material is higher than that of pure MgAlON material. Figure 3b-d reveals that the fracture behavior of MgAlON-MgO composite ceramic (A_3-A_5) transforms into intergranular fracture with the increase of MgO content in the ceramic. This is because the thermal

expansion coefficient of MgAlON (~ 7.4×10^{-6} °C^{-1}) and MgO (13×10^{-6} °C^{-1}) has greatly different, resulting in stress cracks are formed in the grain boundary of the two phases during the sintering process of the MgAlON-MgO ceramic, which reduce the interfacial binding force between MgAlON and MgO phases. As shown in Fig. 3a-d, samples A_3-A_5 have many irregular particles distributed at grain boundaries of the MgAlON-MgO substrate compared with fracture morphology of sample A_2. According to the EDS analysis (Fig. 3e and f) of irregular particles (point 1 and point 2 in Fig. 3b) and XRD result (Fig. 2a) of sample A_3, irregular particles are made up of MgAlON and silicates, respectively.

Figure 4 presents the flexural strength and bulk density of samples A_1-A_5 with different fused magnesite addition. It can be seen that the flexural strength of samples is positively correlated with their bulk density, namely, both change with increase of the fused magnesite addition. The flexural strength and bulk density of sample firstly increase with the fused magnesite addition raised from 12.5% (A_1) to 22.2% (A_2). This may be due to MgO phase promotes grain growth of MgAlON and subsequently reduces porosity of the MgAlON-MgO ceramic. In addition, the fracture behavior of MgAlON-MgO containing 4.2% MgO phase is mainly transgranular fracture, resulting in the increase of the flexural strength. The flexural strength of sample decreases sharply from 172MPa to 89MPa with the fused magnesite addition raised from 22.2% (A_2) to 30% (A_3). Due to the relative content of MgO phase in MgAlON-MgO ceramic raised from 4.2% (A_2) to 14.4% (A_3), stress cracks are formed at the grain boundary between MgAlON and MgO phases, reducing the flexural strength of sample. The result is in agreement with the fracture behavior of the MgAlON-MgO ceramic that changed from transgranular fracture to intergranular fracture. Moreover, compared with the fracture morphology of sample A_2, there are many scattered MgAlON particles and silicate particles on the fracture surface of sample A_3. Combined with the changing trend of the bulk density of samples A_2-A_3 in Fig. 3, these irregular particles enriched at grain boundaries of the MgAlON-MgO substrate cause the small density change of the ceramic. The flexural strength of the MgAlON-MgO ceramic remain stable when the fused magnesite addition exceeded 30% (A_3-A_5), indicating that the increase of the MgO content in the ceramic does not worsen the interfacial binding force between MgAlON and MgO phases as the relative content of MgO phase exceeds 14.4%. In conclusion, when the MgO phase content in MgAlON-MgO composite ceramic is 4.2%, the flexural strength of the composite ceramic reaches the maximum value of 172MPa.

Table 3 reveals the comparison of flexural strength and synthetic parameter obtained in this study with those of ceramic-based friction materials. Heidenreich et al.[4] synthesized C/C-SiC friction material with flexural strength of 132MPa by hot-press shaping at 250℃, pyrolysis exceeded 900℃ and pressureless sintering at 1400℃. Tang et al.[7] prepared C_{sf}/SiC friction material with flexural strength of 466MPa by hot-press sintering at 1800℃. However, the complex synthetic process and the high production cost hinder the application of those friction materials. Hence, the MgAlON-MgO ceramic prepared by in-situ pressureless sintering at 1600℃ with 11.1% spent MgO-C brick utilization rate behaves excellent mechanical properties, low cost and simple synthetic process, exhibiting a great competitive advantage to be applied for the friction material of automobile brake blocks.

Table 3
Comparison of flexural strength and synthetic parameter for several ceramic-based friction materials

Ceramics	Flexural strength (MPa)	Synthetic parameter			Reference
		Pretreatment processing	Sintering processing	Sintering temperature (℃)	
C/C-SiC	132	Hot-press shaping (250℃), Pyrolysis (T > 900℃)	Pressureless sintering	1420	[4]
C/C-SiC	186	Twice hot-press curing (120℃ and 180℃), Pyrolysis (1000℃)	Pressureless sintering	1450	[6]
C_{sf}/SiC	466	-	Hot-press sintering (25MPa)	1800	[7]
MgAlON-MgO	172	Cold-press shaping	Pressureless sintering	1600	This work

3.3. Preparation of high strength MgAlON-MgO refractory

In order to reduce the production cost of MgAlON-MgO ceramic and improve the utilization rate of spent MgO-C brick, the effect of the spent MgO-C brick addition on the phase composition, microstructure and flexural strength of the MgAlON-MgO composite material was studied.

According to Table 2, the green bodies B_1-B_5 were calcined at 1600℃ for 3h under flowing nitrogen atmosphere. The XRD patterns of specimens B_1-B_5 and the relative contents of MgAlON phase and MgO phase are shown in Fig. 5a and b, respectively. The samples B_1-B_5 are confirmed to be MgAlON-MgO composite material on the basis of XRD patterns (Fig. 5a). As shown in Fig. 5b, the relative content of MgO phase in the MgAlON-MgO composite material increases with the raise of spent MgO-C brick addition. Figure 5c shows the MgO content variation before and after sintering for A and B series from different magnesium source. The MgO content of the green body was calculated according to the chemical composition of raw materials in Table 1, and the MgO content of the sample after sintering was obtained from Fig. 2b and Fig. 5b. It can be seen from Fig. 5c that the MgO content after sintering increases with the raise of MgO content before sintering for both A and B series. However, the difference of MgO content after and before sintering for series A decreases with the increase of the MgO content in green body, while it is opposite for series B. This is because the increase of spent MgO-C brick addition raises the MgO content in the green body while also raising the carbon content in the green body, promoting the degree of carbothermal reduction and nitridation reaction and increasing the generation of the MgAlON phase. Therefore, compared with the A series using fused magnesite as the main magnesium source, the B series using the spent MgO-C brick as the main magnesium source improve the formation of MgAlON phase which play a positive role in the resistance to bending load of MgAlON-MgO composite ceramic.

The fracture morphologies of the samples B_2-B_5 with different spent MgO-C brick addition are shown in Fig. 6. It can be found that the fracture behavior of samples B_2-B_5 is intergranular fracture and the pore size increases with the raise of spent MgO-C brick addition. The reason is that the raise of the spent MgO-C brick addition increases the carbon content in the green body, enhancing the formation amount of gas phase such as carbon monoxide (CO) and carbon dioxide (CO_2) generated by carbothermal reduction and nitridation reaction during the sintering process. Moreover, compared with the fracture morphologies of specimens A_3-A_5, the fracture surface of composite material with spent MgO-C brick as the main magnesium source does not be observed irregular particles composed of silicate phase. Hence, the impurity introduced by the spent MgO-C brick may exist in MgAlON-MgO substrate.

In order to determine the distribution of MgAlON and MgO phases, and the form of impurity phases introduced by spent MgO-C brick in MgAlON-MgO composite material, the sample B_5 was analyzed by backscattering analysis and transmission electron microscope analysis. Figure 7 reveals the backscattered electron morphology of cross-section and the mapping photos of determining elements C, O, Mg, Al, Fe, Si and Ca for sample B_5. The grey zone (GZ) in Fig. 7a is mainly consist of elements Mg, Al and O, while the dark grey zone (DGZ) in Fig. 7a is mainly made up of elements Mg and O. Combined with the XRD pattern of the sample B_5, the GZ and the DGZ are deduced as MgAlON and MgO, respectively. Due to MgAlON phase contains extra Al element compared with MgO phase, it can be determined that MgAlON is a continuous phase and MgO phase is uniformly distributed in the MgAlON matrix according to distribution of Mg and Al elements in the Fig. 7d and e. In addition, the black zone (BZ) in Fig. 7a is mainly composed of element C. Certainly, the determined element C is produced by spraying carbon on the surface of the sample before SEM analysis. As shown in Fig. 7f-h, the impurity elements Fe, Si and Ca are uniformly distributed in the matrix.

Figure 8a-f reveals the TEM morphology and the mapping photos of determining elements Mg, O, Si, Ca and Fe for sample B_5. It can be seen that region A is composed of Mg, Ca, Si and O elements, region B is made of Mg and O elements, and region C is composed of Fe, Mg and O elements. The selected area electron diffraction of region 1, region 2 and region 3 (Fig. 8a) are shown in Fig. 8g-i, respectively. By calibrating the diffraction pattern, regions 1–3 are determined to be $CaMgSiO_4$, $MgFe_2O_4$ and MgO, respectively. Combined with the mapping photos of elements in Fig. 8b-f, regions A, B and C in Fig. 8a are $CaMgSiO_4$, MgO and $MgFe_2O_4$, respectively.

Figure 9 shows the flexural strength and bulk density of sintered samples B_1-B_5. The flexural strength and bulk density of samples B_1-B_5 decrease with the increase of spent MgO-C brick addition. When the utilization ratio of spent MgO-C brick reaches 52.9%, the flexural strength and bulk density of MgAlON-MgO composite material reach 46MPa and 2.26g/cm^3, respectively. It is well known that pores play a negative role on the mechanical properties of material. As shown in Fig. 6, the pore size increases with the rise of the spent MgO-C brick addition, which explains why the flexural strength and bulk density of those specimens decreases with the raise of spent MgO-C brick addition. In addition, Fig. 5b presents that MgAlON content in MgAlON-MgO composite material reduces with the rise of spent MgO-C brick addition,

which is another reason for the decrease of flexural strength of samples. According to the analysis of selected area electron diffraction and standardization for the sample B_5, it can be found that impurities introduced by spent MgO-C brick exist in the form of $CaMgSiO_4$ and $MgFe_2O_4$. The low melting point phase $CaMgSiO_4$ (melting point 1498℃[22]) distributed in the MgAlON-MgO (seen Fig. 7g and h) substrate melts and exists in the form of liquid phase during high temperature sintering process, which can benefit to the density of the composite material and subsequently improve the flexural strength of the material. Figure 8a shows that $MgFe_2O_4$ is embedded in MgO phase. Due to the thermal expansion coefficient of $MgFe_2O_4$ (11.5×10^{-6} ℃$^{-1}$[23]) is similar to that of MgO (13×10^{-6} ℃$^{-1}$), there is not stress crack at the grain boundary between the two phases, indicating that $MgFe_2O_4$ has no obvious effect on the bulk density and flexural strength of the MgAlON-MgO composite material.

Comparison of flexural strength and synthetic parameter for several MgAlON combined refractory are shown in Table 4. Yang et al.[13] prepared MgAlON-MgO composite material by pressureless sintering at 1500℃ for 6h used metal aluminum powder, alumina micro powder and fused magnesia as raw materials, and its flexural strength reached 10MPa. The MgAlON-MgO composite material prepared from spent MgO-C brick in this work has higher flexural strength and lower production cost than that of MgAlON-MgO composite material from pure raw materials, which may be that the impurities from spent MgO-C brick generate low melting phase at high temperature improves the interfacial binding force between MgAlON and MgO phases. Chen et al.[24] obtained MgAlON-Al_2O_3 composite material with flexural strength of 7.7MPa from Al_2O_3 powder, spent MgO-C and Al_2O_3-MgO-C bricks at 1550℃ for 6h, while the addition amount of spent bricks was 54%. The flexural strength of MgAlON-MgO in this work also is better than that of MgAlON-Al_2O_3 under the same utilization rate of spent bricks. In conclusion, the in-situ synthesized MgAlON-MgO composite material with 52.9% spent MgO-C brick addition is expected to be used as refractory material for high temperature industries such as steel, cement, and glass production due to its excellent flexural strength and low production cost.

Table 4
Comparison of flexural strength and synthetic parameter for several MgAlON combined refractory

Refractory	Synthetic parameter			Flexural strength (MPa)	Reference
	Raw material	Sintering temperature (°C)	Soaking time (h)		
MgAlON-MgO	Metal aluminum powder, Alumina micro-powder, Fused magnesite	1500	6	10	[13]
MgAlON - $MgAl_2O_4$	Metal aluminum powder, Alumina micro-powder, Fused spinel ($MgO{\cdot}Al_2O_3$)	1500	6	19	[13]
MgAlON - Al_2O_3	Spent MgO-C brick, Spent Al_2O_3-MgO-C brick, Al_2O_3 powder	1550	4	7.7	[24]
MgAlON-MgO	Spent MgO-C brick, Alumina micro-powder, Fused magnesite	1600	3	46	This work

4. Conclusion

The MgAlON-MgO ceramics with different flexural strength were in-situ synthesized by pressureless sintering from spent MgO-C brick at 1600℃ for 3h in nitrogen atmosphere. MgAlON is continuous phase in the ceramic, and the MgO phase is uniformly distributed in the MgAlON matrix. The maximum flexural strength and bulk density of the MgAlON-MgO ceramic with 11.1% spent MgO-C brick addition reach 172MPa and 3.169g/cm^3, respectively, which is expected to be applied for the friction material of automobile brake blocks due to its high mechanical strength, simple synthesis process and low production cost. In addition, when the utilization rate of spent MgO-C brick is increased to 52.9%, the flexural strength of MgAlON-MgO ceramic still reaches 46MPa, which is expected to be used as refractory material for high temperature industries such as steel, cement, and glass production.

The flexural strength and bulk density of MgAlON-MgO ceramic decrease with the increase of the spent MgO-C brick addition. The C, MgO and Al_2O_3 in spent MgO-C brick are used as reactants to participate carbothermal reduction nitridation reaction for generation of MgAlON phase. However, the pore caused by the generation of CO and CO_2 during reaction process reduces the density of MgAlON-MgO ceramic. So, the C contributes negatively to flexural resistance. The impurity phases CaO, Fe_2O_3, and SiO_2 introduced by the spent brick exist at the composite ceramic in the form of $CaMgSiO_4$ and $MgFe_2O_4$, respectively. The low melting phase $CaMgSiO_4$ increases the density of the composite material, indicating that the impurities CaO and SiO_2 play a positive role in the resistance to bending load. And $MgFe_2O_4$ has no obvious effect on the bulk density and flexural strength of the MgAlON-MgO composite material.

Declarations

Acknowledgements

This research was funded by the National Natural Science Foundation of China (51972019, U1810205, 51672025).

References

1. Chan D, Stachowiak GW (2004) Review of automotive brake friction materials. Proc Inst Mech Eng Part D 218:953–966
2. Kermc M, Kalin M, Vižintin J (2005) Development and use of an apparatus for tribological evaluation of ceramic-based brake materials. Wear 259:1079–1087
3. Krenkel W, Heidenreich B, Renz R (2002) C/C-SiC composites for advanced friction systems. Adv Eng Mater 4:427–436
4. Heidenreich B, Renz R, Krenkel W (2001) Short Fibre Reinforced CMC Materials for High Performance Brakes. In: Krenkel W, Naslain R, Schneider H (eds) High Temperature Ceramic Matrix Composites. Wiley, Stuttgart, pp 809–815
5. He XL, Zhou Y, Jia DC et al (2006) Effect of sintering additives on microstructures and mechanical properties of short-carbon-fiber-reinforced SiC composites prepared by precursor pyrolysis–hot pressing. Ceram Int 32:929–934
6. Yang JH, Ai YJ, Lv XX et al (2020) Fabrication of C/C-SiC composites using high-char-yield resin. Int J Appl Ceram Technol 18:449–456
7. Tang HL, Zeng XR, Xiong XB et al (2007) Effect of short carbon fiber content on the mechanical properties of composite Csf/SiC. J Chin Ceram Soc 35:1057–1061
8. Zhang HX, Hong YR, Huang Y et al (2005) Precise determination of the MgAlON/(AlN + MgAlON) phase boundries in the MgO-AlN-Al_2O_3 ternary system at 1600^{o}C and 1700^{o}C. J Mater Sci Technol 21:277–280
9. Zhang ZT, Teng LD, Li WC (2007) Mechanical properties and microstructures of hot-pressed MgAlON–BN composites. J Eur Ceram Soc 27:319–326
10. Dai WB, Yamaguchi A, Lin W et al (2007) Preparation and properties of spark plasma sintered magnesium aluminum oxynitride. J Ceram Soc Jpn 115:525–529
11. Wang XD, Wang FM, Li WC (2003) Synthesis thermodynamics and properties of MgAlON ceramics. J Inorg Mater 18:83–90
12. Cheng Z, Sun JL, Wu XZ et al (2011) Microstructure and properties of MgAlON-bonded magnesia, magnesia-alumina spinel and corundum materials. J Univ Sci Technol B 33:1378–1386
13. Yang DY, Zhang HY, Zhong XC (2006) Study on preparation and mechanical property of MgO-$MgAl_2O_4$-MgAlON composites. Naihuo Cailiao 40:12–15
14. Wang XT, Wang HZ, Zhang BG et al (2005) Sintering property of MgAlON bonded composite materials. Naihuo Cailiao 39:22–25

15. Wu XW, Chi P, Cheng BH et al (2020) Research and development of recycling utilization of used refractories: a review. China's Refract 29:38–47
16. Li HX (2018) Development overview of refractory materials. J Inorg Mater 33:198–205
17. Ewais EMM (2004) Carbon based refractories. J Ceram Soc Jpn 112:517–532
18. Arianpour F, Kazemi F, Golestani-Fard F et al (Characterization of spent MgO-C refractory bricks with emphasise on recycling. In: Unified International Technical Conference on Refractories 2007) Dresden, 2007: 598–601
19. Avelar TC, Veiga AF, Gueguen E et al (2012) Recycling practices of crushed MgO-C bricks and dolomite sinter fines used as a slag conditioning additive in the EAF. Waste Manage Environ VI 163:259–270
20. Cheng X, Liu L, Qiu GB et al (2020) Low temperature and pressureless synthesis of MgAlON: qualitative analysis and formation evolution. Int J Mater Res 111:537–545
21. Dai WB, Lin W, Yamaguchi A et al (2007) Synthesis of magnesium aluminum oxynitride by carbothermal reduction and nitridation process. J Ceram Soc Jpn 115:42–46
22. Moshtaghioun BM, Monshi A (2008) Analyze complex phases of slag–tundish plaster reactions by modified XRD ratio of slopes method for some kinetic considerations. J Mater Process Technol 196:52–63
23. Carter RE (1959) Thermal expansion of $MgFe_2O_4$, FeO, and MgO·2FeO. J Am Ceram Soc 42:324–327
24. Chen WB, Wang B, Liu LL et al (2020) Preparation and slag erosion resistance mechanism of MgAlON based composite refractories synthesized from solid waste. Ceram Int 46:26035–26043

Figures

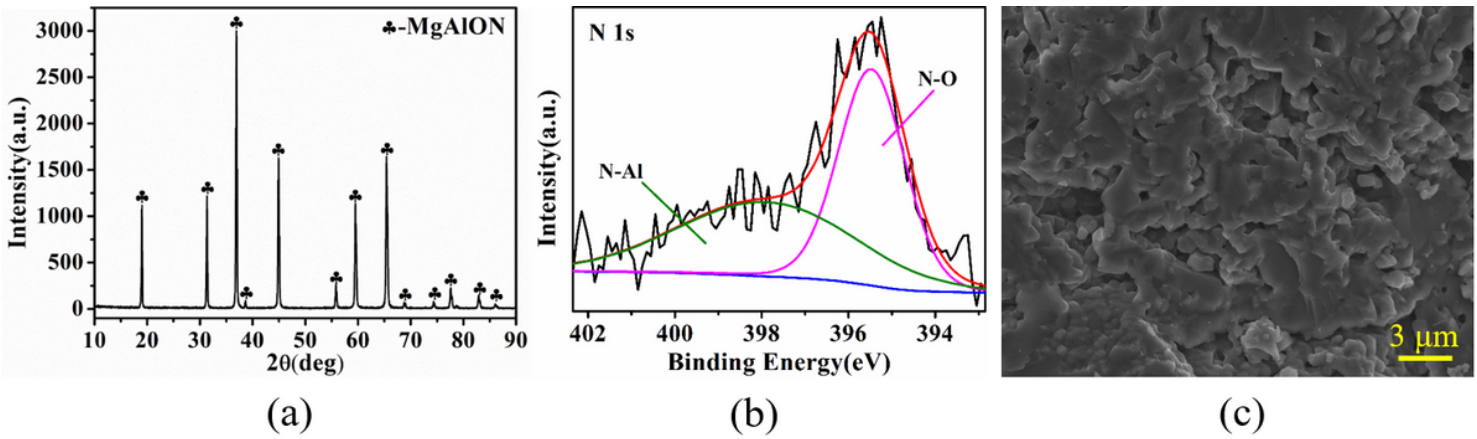

Figure 1

(a) The XRD pattern, (b) the N 1s XPS spectra and (c) the fracture morphology of the sample A1.

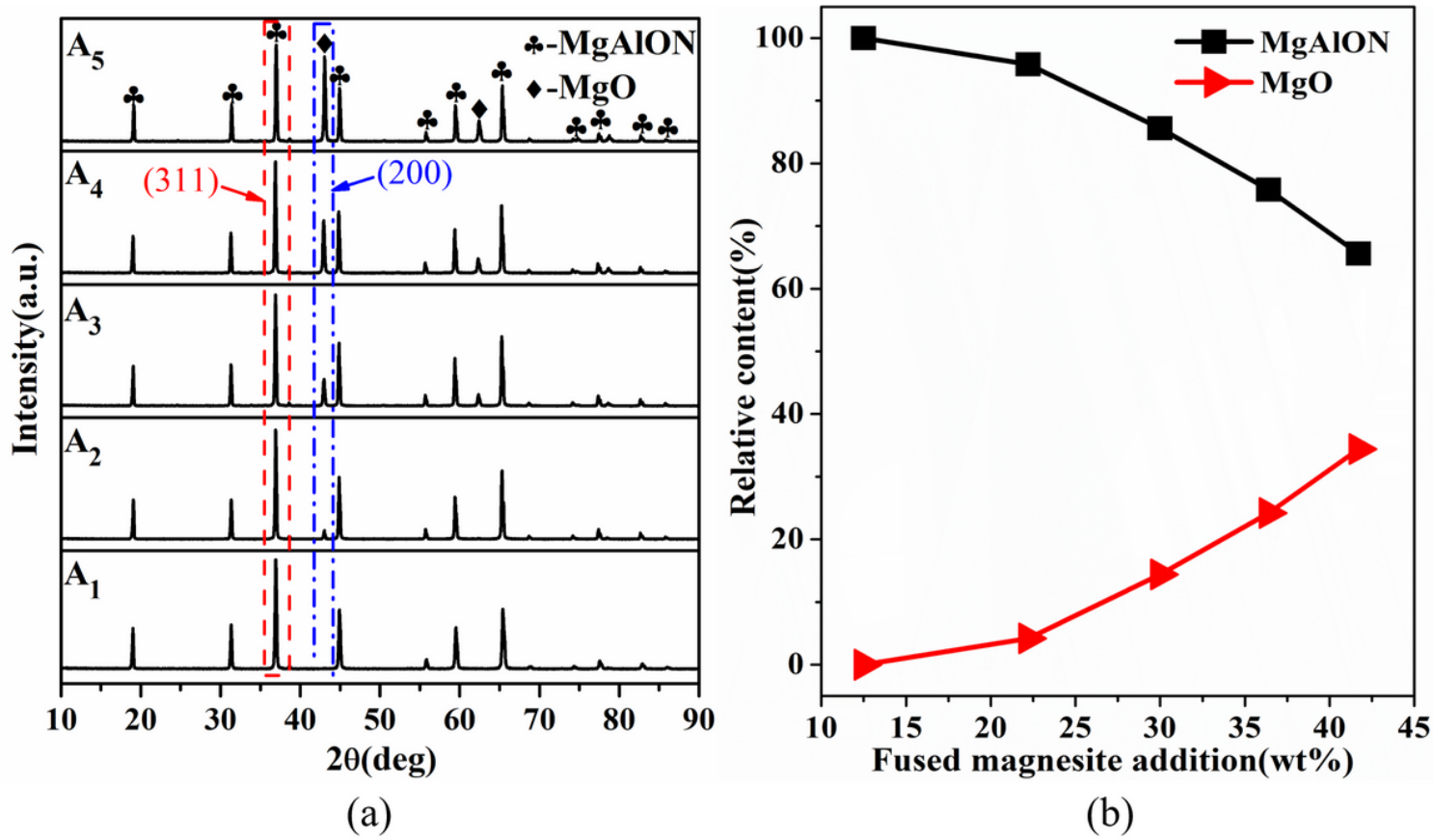

Figure 2

(a) The XRD patterns and (b) the relative contents of MgAlON and MgO phases in specimens (A1-A5) with different fused magnesite addition.

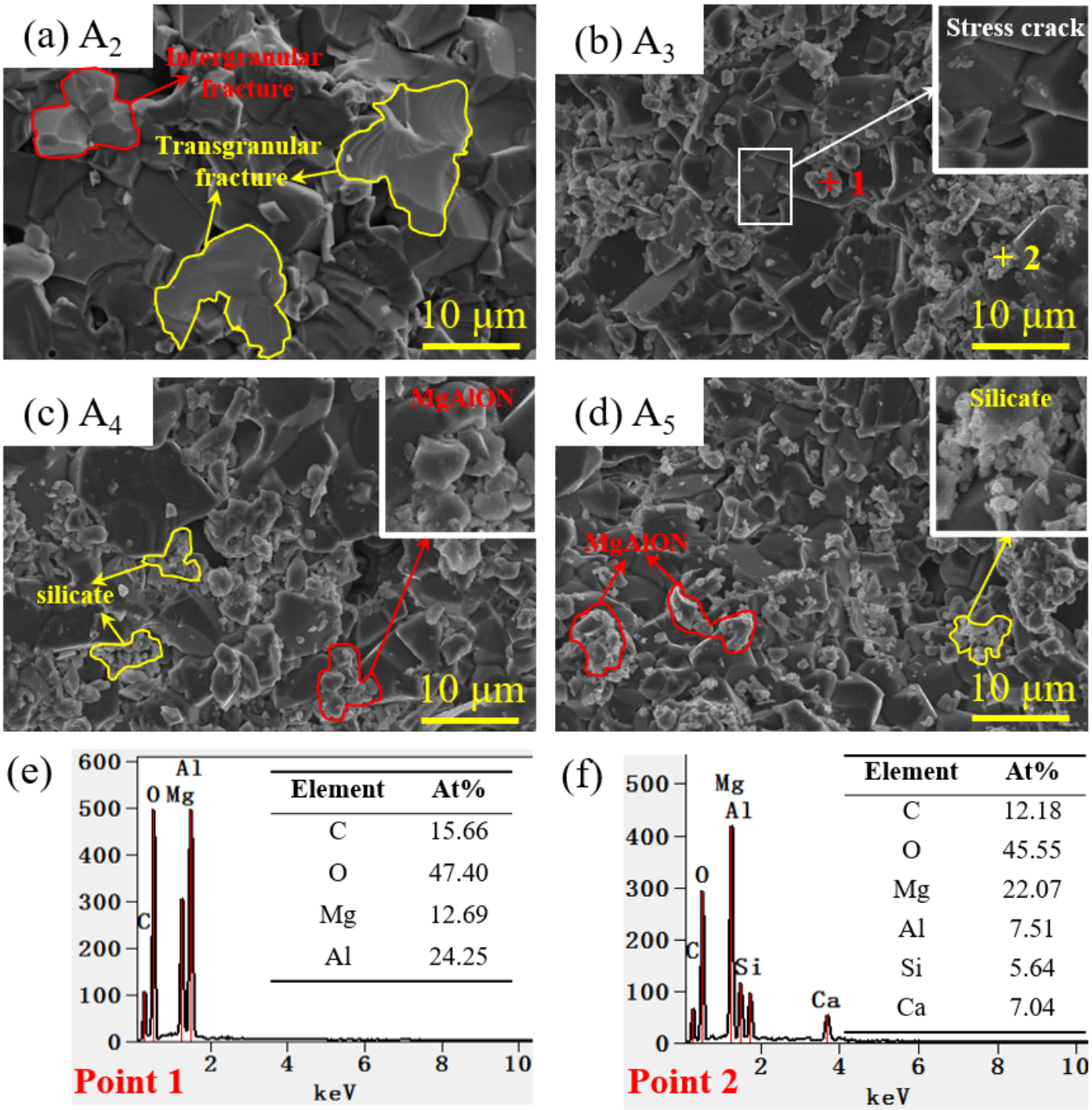

Figure 3

(a-d) The fracture morphologies of specimens (A2-A5) with different fused magnesite addition and (e-f) EDS result of specimen A3.

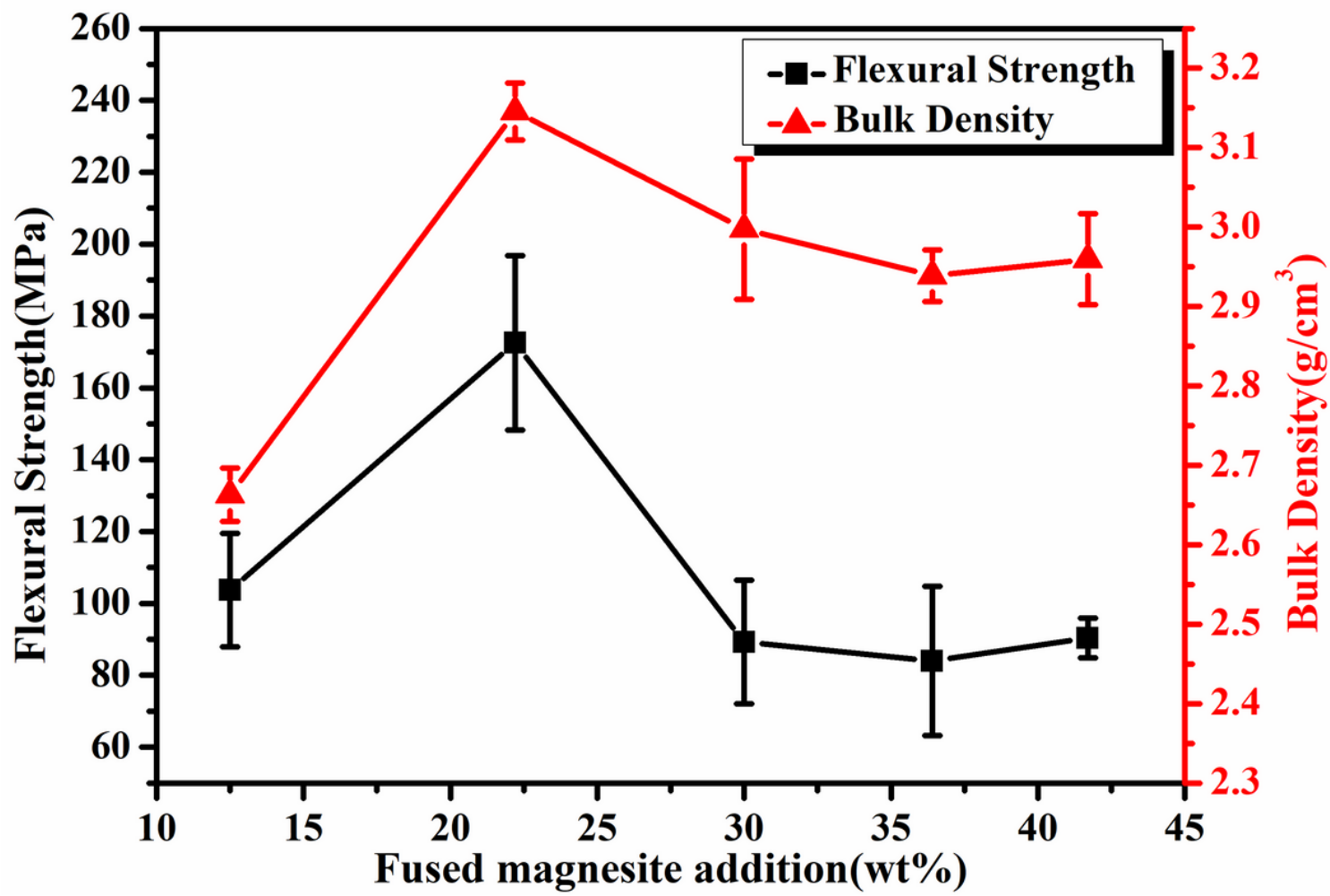

Figure 4

The flexural strength and bulk density of specimens (A1-A5) with different fused magnesite addition.

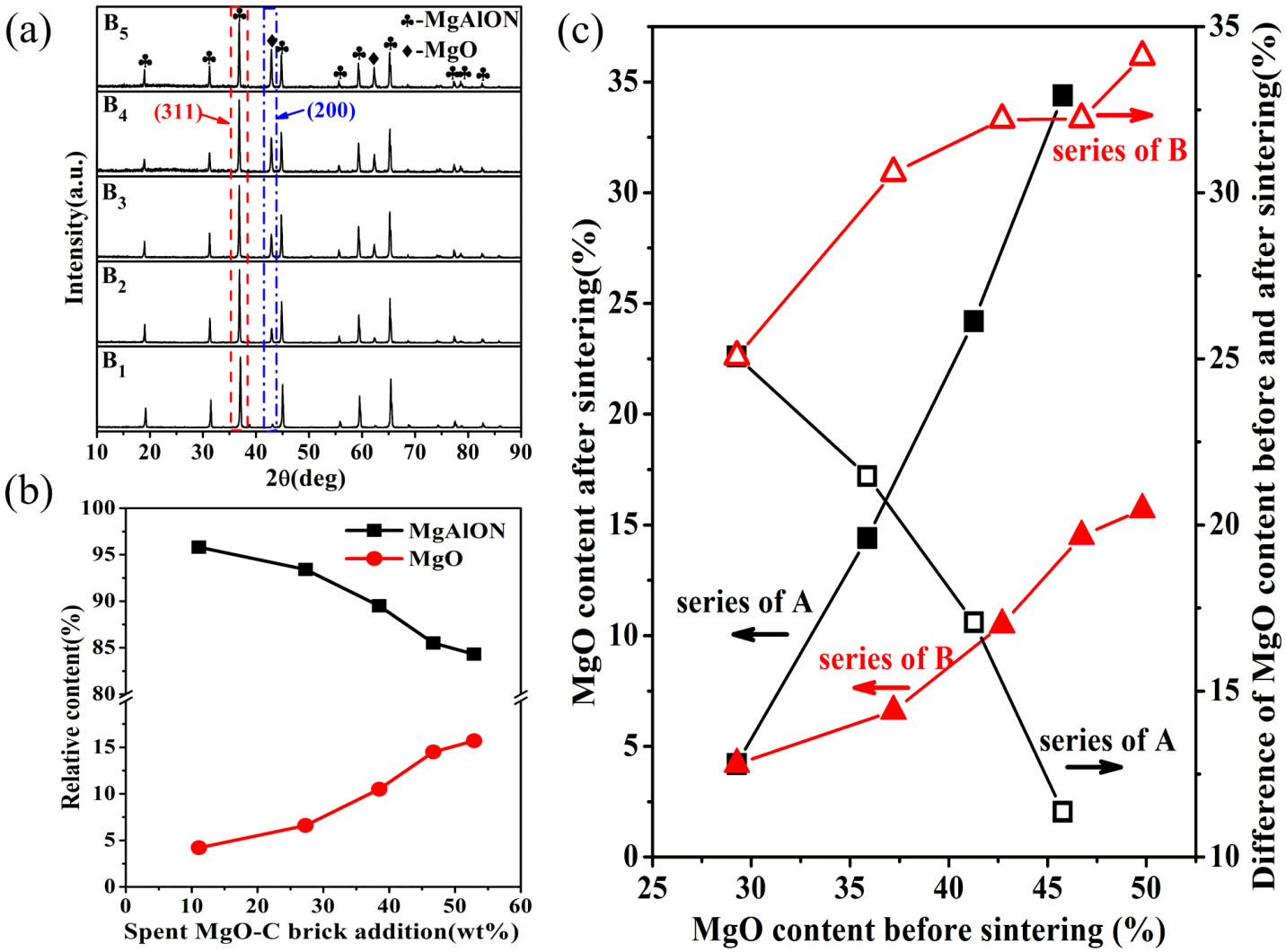

Figure 5

(a) The XRD patterns and (b) the relative contents of MgAlON and MgO phases in specimens (B1-B5) with different spent MgO-C brick addition, (c) MgO content variation before and after sintering for A and B series.

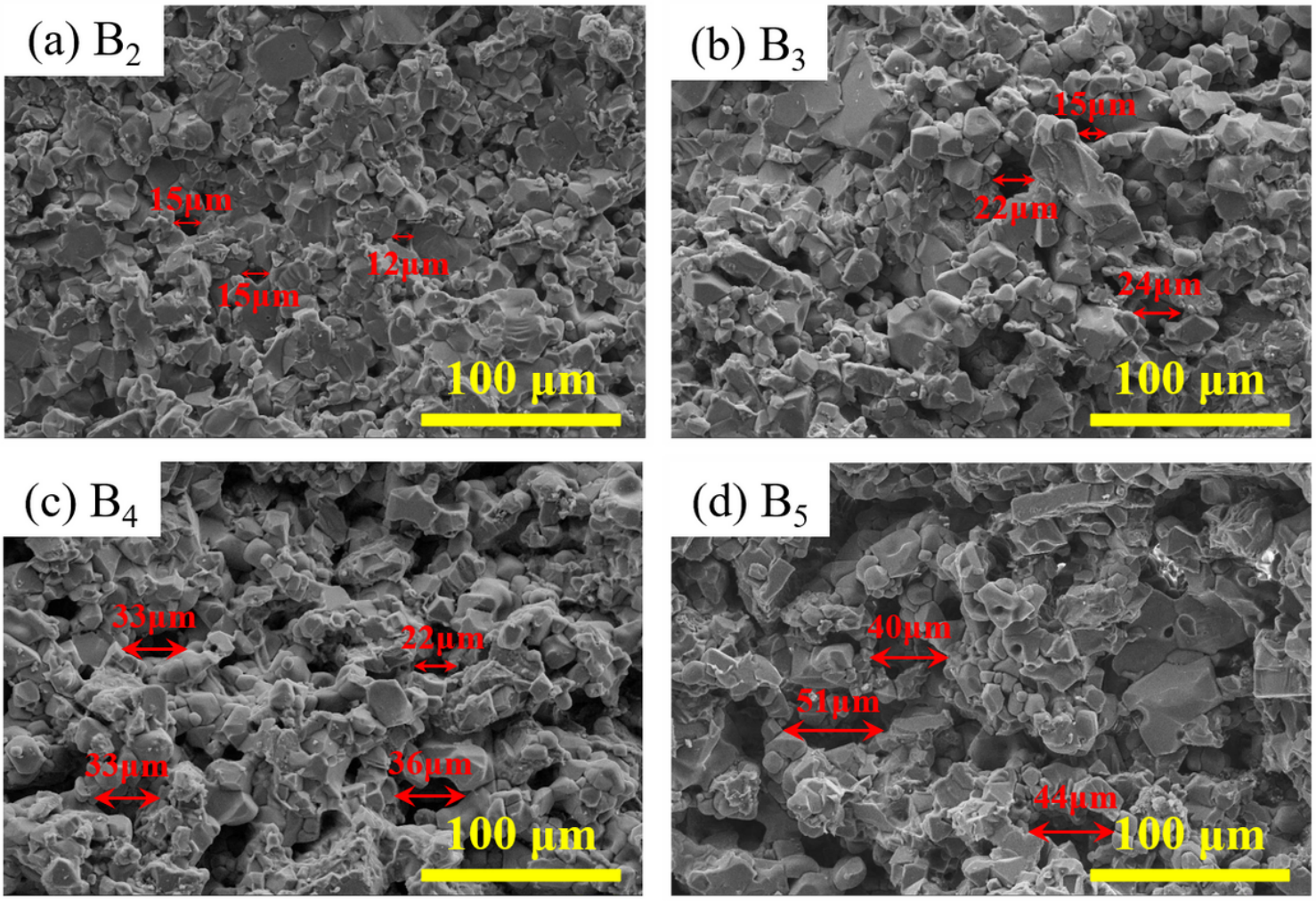

Figure 6

The fracture morphologies of specimens (B2-B5) with different spent MgO-C brick addition.

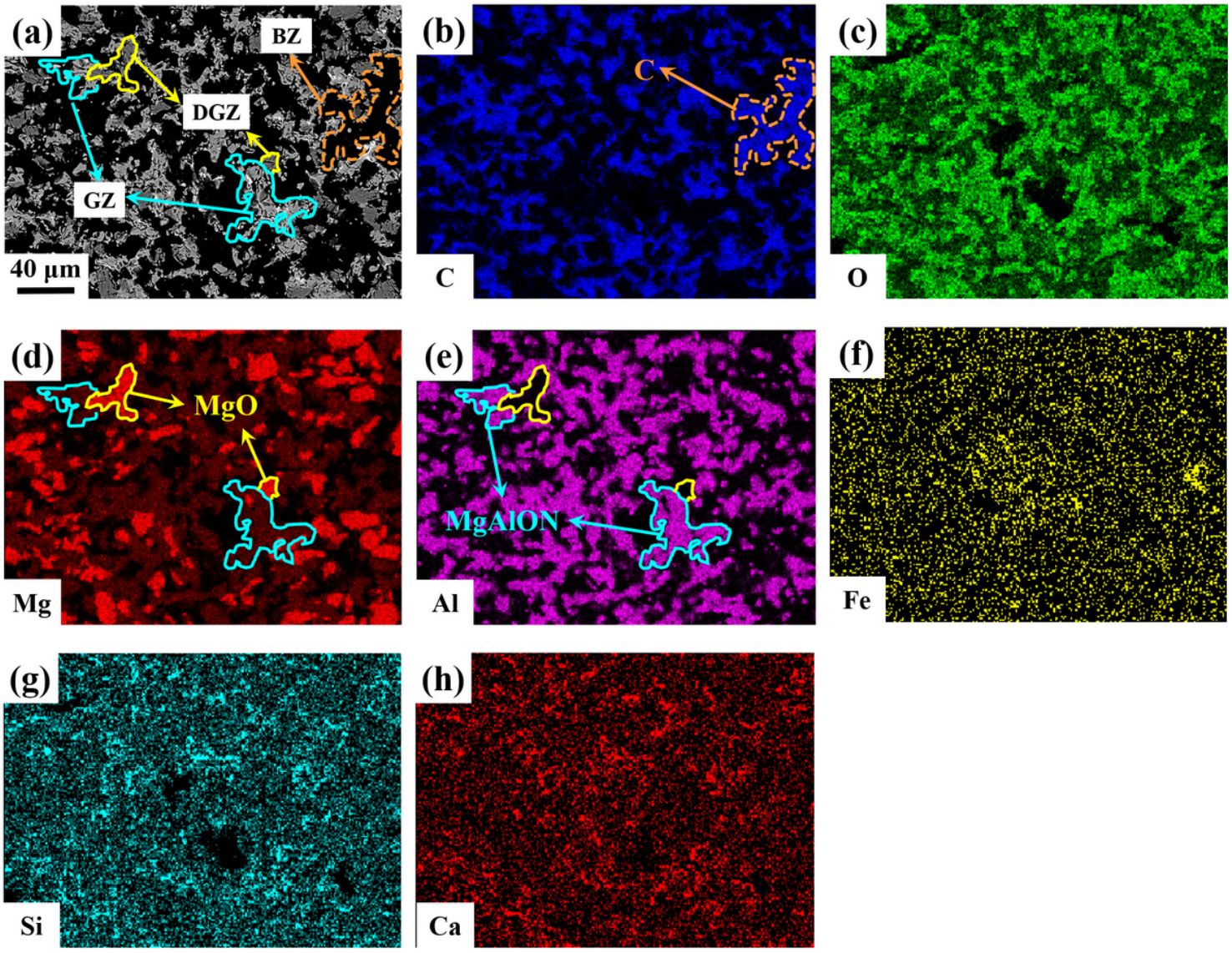

Figure 7

(a) Backscattered electron morphology of cross-section and (b-h) the mapping photos of determining elements C, O, Mg Al, Fe, Si and Ca for the sample B5.

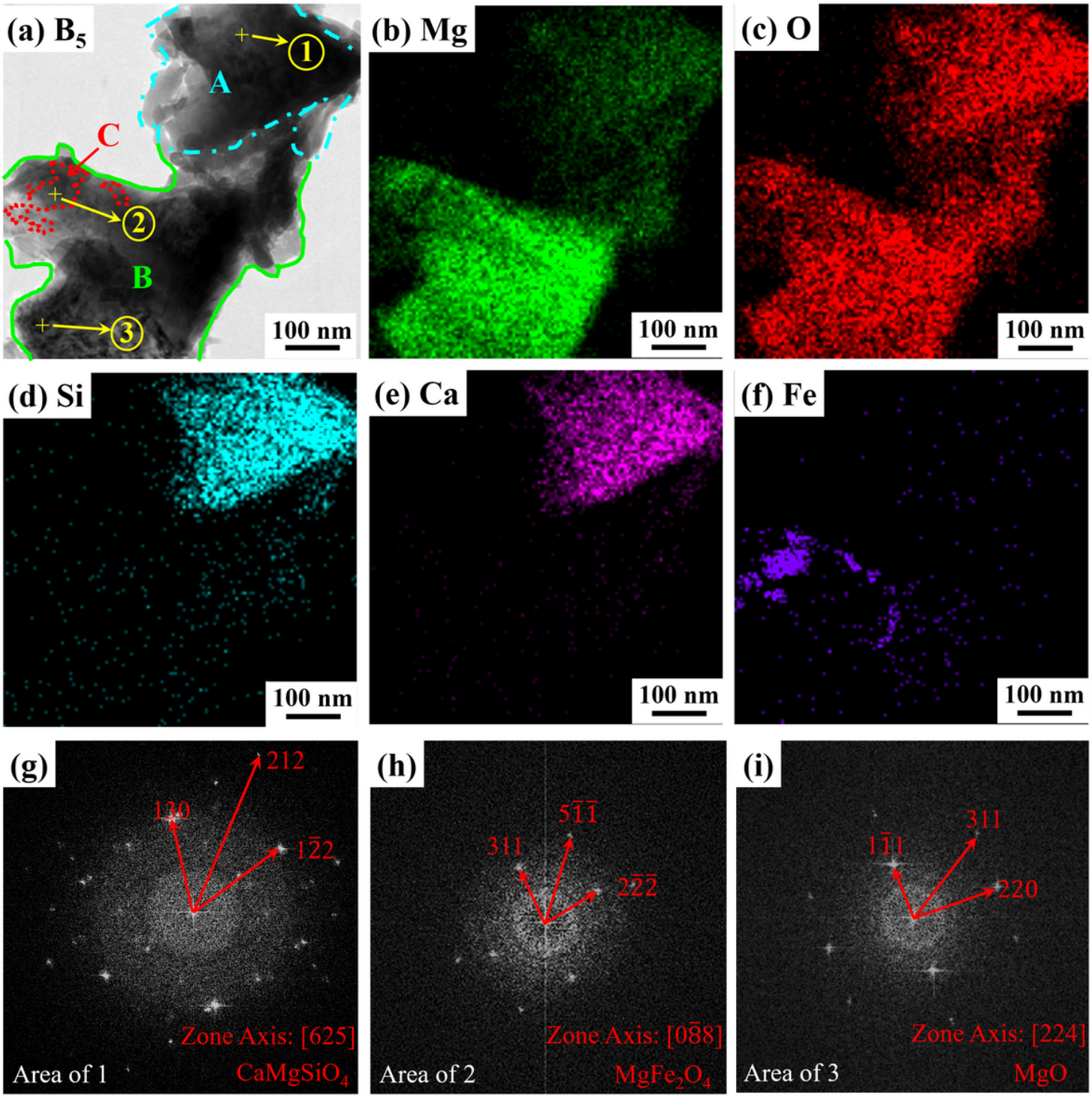

Figure 8

(a) TEM morphology, (b-f) the mapping photos of determining elements Mg, O, Si, Ca and Fe, (g-i) selected area electron diffraction and standardization for the sample B5.

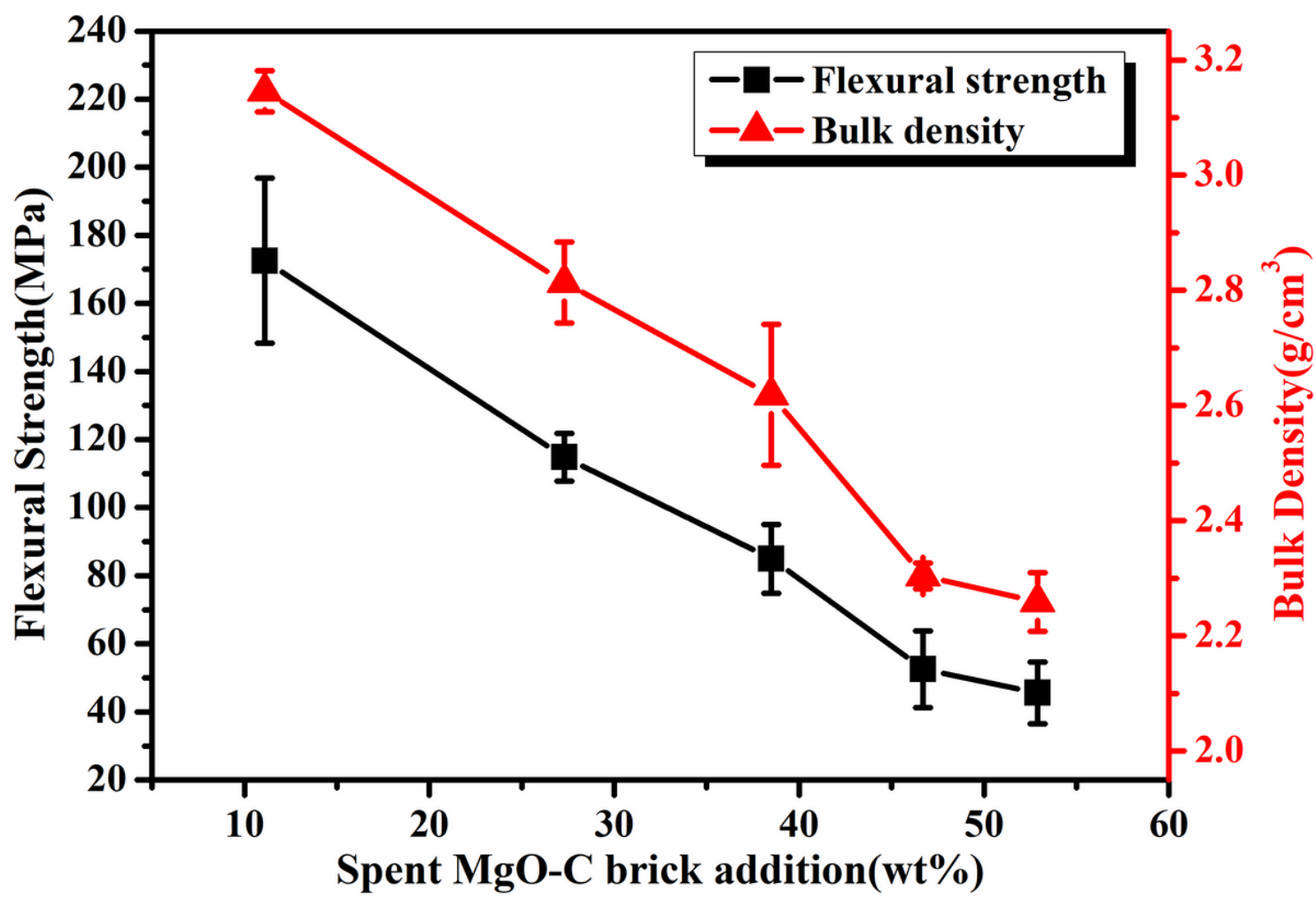

Figure 9

The flexural strength and bulk density of specimens (B1-B5) with different spent MgO-C brick addition.